

PAPER

## Theoretical study on the thermal transport and its tunability of a-plane trilayer GaN

To cite this article: Yaxin Xu *et al* 2023 *Phys. Scr.* **98** 065944

View the [article online](#) for updates and enhancements.



### You may also like

- [Electrical transport mechanism and magnetoresistive behavior of trilayer  \$\text{La}\_{0.7}\text{Sr}\_{0.3}\text{MnO}\_3/\text{Fe}\_2\text{O}\_3/\text{La}\_{0.7}\text{Sr}\_{0.3}\text{MnO}\_3\$  \(FM/FIM/FM\) manganites](#)  
Pooja Narwat, R J Choudhary and A Mishra
- [Regulation of depletion layer width in  \$\text{Pb}\(\text{Zr,Ti}\)\text{O}\_3/\text{Nb:SrTiO}\_3\$  heterostructures](#)  
Yu Bai, Zhān Jie Wang, Jian Zhong Cui et al.
- [FMR-driven spin pumping in  \$\text{Y}\_3\text{Fe}\_5\text{O}\_{12}\$ -based structures](#)  
Fengyuan Yang and P Chris Hammel



## PAPER

## Theoretical study on the thermal transport and its tunability of a-plane trilayer GaN

RECEIVED  
21 December 2022REVISED  
27 April 2023ACCEPTED FOR PUBLICATION  
5 May 2023PUBLISHED  
17 May 2023Yaxin Xu, Guoqing Sun, Zijing Wan, Dongwei Xu\*  and Xiaobing Luo 

School of Energy and Power Engineering, Huazhong University of Science and Technology, Wuhan, Hubei 430074, People's Republic of China

\* Author to whom any correspondence should be addressed.

E-mail: [dwxu@hust.edu.cn](mailto:dwxu@hust.edu.cn)**Keywords:** thermal conductivity, strain engineering, 2D GaNSupplementary material for this article is available [online](#)**Abstract**

Two-dimensional (2D) a-plane gallium nitride, a non-layered 2D material, has promising applications in photoelectric nanodevices due to its direct band bandgap. Herein, employing molecular dynamics simulations, we studied the thermal transport properties of a-plane trilayer GaN, and the temperature, together with strain modulation on the thermal conductivity of the system. The a-plane trilayer GaN shows anisotropic thermal conductivity with  $70.22 \text{ Wm}^{-1}\text{K}^{-1}$  and  $41.81 \text{ Wm}^{-1}\text{K}^{-1}$  along zigzag- and armchair- directions respectively at room temperature when extrapolated to infinite size. In addition, the thermal conductivity of trilayer GaN exhibits decreasing trend in response to the increase of temperature. The thermal conductivity decreases monotonically with the increased compressive uniaxial and biaxial strain, while it shows an up-then-down trend under tensile strain. The tunability of thermal conductivity under biaxial strain is much larger than that of uniaxial strain. The phonon density of states is further investigated to understand the behavior of thermal conductivity. The tunability of the system thermal conductivity will expand its applications in thermal management and nanodevices.

**1. Introduction**

Gallium nitride (GaN), a typical non-layered material, its excellent electronic and optical properties [1–3] have made it an important wide bandgap semiconductor with wide ranging technological applications in light-emitting diodes (LEDs) [1], laser diodes [4, 5], solar cells [6] and microwave power transistors [7]. Motivated by the emergence of two-dimensional (2D) materials with unique optical, electrical, and mechanical properties [8–13], and the successful fabrication of the 2D materials [14], 2D GaN has attracted much attention [15–18]. There are four typical forms of GaN 2D films [19]: the polar c-plane along (0001), the nonpolar m-plane along  $(10\bar{1}0)$ , the nonpolar a-plane along  $(1\bar{2}10)$ , and the semipolar r-plane along  $(11\bar{2}2)$  [19]. With the structural changes brought about by the reduction of a material from 3D to 2D, its physical properties also change. In terms of the monolayer (ML) GaN, it is confirmed that the stable GaN monolayer exhibits a hexagonal planar structure in both the polar c-plane GaN and the nonpolar m-, a-plane [5, 19]. However, in contrast to conventional 2D layered materials such as graphene, transition-metal dichalcogenides [20], whose 2D ML structures exhibit direct bandgap while the corresponding 3D materials show indirect bandgap, ML GaN has an indirect bandgap [19] when the dimension is reduced from bulk with direct bandgap. The indirect bandgap of material limits its further application in optical-electronic devices due to the decreased photoelectric conversion efficiency. Cai *et al* explored multilayer m-plane GaN, which shows an indirect bandgap from 1 ML to 11 ML by density functional theory calculations [19]. For the multilayers c-plane GaN, A V Kolobov *et al* proposed an 8/4 heackelite configuration which is comprised of alternating octagonal and square rings, and manifest as direct bandgap only from 2 ML to 4 ML [21]. However, our previous work on a-plane GaN with layers greater than two showed that it has a direct band gap that is beneficial for optoelectronic applications.

It is worth noting that the thermal transport property of material is an important factor affecting the performance of photo-electric applications. Low thermal conductivity will cause the heat accumulation and may damage the device, which limits the application of device. Much attention has been paid to modulate thermal conductivity in the past few decades. Strain engineering is proved to be an effective way to turn thermal conductivity. In addition, strain is unavoidable during the fabrication of 2D materials due to lattice mismatch with the substrate, and the working process due to thermal expansion. For the 2D layered structure, the thermal conductivity of  $C_3N_3$  and  $C_3N_7$  can be greatly enhanced at uniaxial tensile strain of 4% and 2%, respectively, while slightly decreases under uniaxial compressive strain [22]. The thermal conductivity of  $C_3N$  monolayer and bilayer shows monotonic decrease under uniaxial and biaxial tensile strain [23]. For 2D hexagonal boron nitride [24],  $BN_3$  [25] and  $BC_2N$  [26], the thermal conductivity shows a monotonic decrease trend under compressive strain while an up-then-down trend is introduced by the tensile strain. The thermal conductivity of other material decreases continuously when the strain changes from compressive to tensile such as silicon 2D film [27]. It can be seen that the modulating effect of strain on 2D materials depends mainly on the material and structure. To explore the modulation of thermal conductivity and to broaden the application of GaN, we will explore the modulation effect of strain on thermal conductivity of a-plane trilayer GaN (3L-GaN).

In this work, we investigated the thermal transport of the nonpolar a-plane 3L-GaN by performing molecular dynamics (MD) simulations. The size and temperature effect, together with the modulation of uniaxial and biaxial strain, are well studied. The results will extend the modulating range of the thermal conductivity for different application purpose.

## 2. Simulation method

The lattice structure of the nonpolar a-plane 3L-GaN is shown in figure 1 and the simulation system is shown in figure 2(a). The primitive unit cell contains 12 atoms and the in-plane lattice parameters are  $a = 5.56 \text{ \AA}$  and  $b = 5.23 \text{ \AA}$  respectively. A vacuum of  $20 \text{ \AA}$  is added along  $c$  direction to avoid the interaction between upper and lower layers. The thickness of the structure,  $6.628 \text{ \AA}$ , which is the distance between the top layer and the bottom layer plus the van der Waals diameter of Ga [29], is used to calculate the cross-sectional area and then to calculate the thermal conductivity.

All the molecular dynamics (MD) simulations are performed by using the Large-scale Atomics/Molecular Massively Parallel Simulator (LAMMPS) package [30]. The interactions between Ga and N atoms are described by the Stillinger-Weber (SW) potential parametrized by Bér e *et al* [31]. The SW potential complements the usual pair-wise interaction terms with three-body angularly-dependent terms that stabilize these crystal structures, and can accurately describe Ga-N interactions. The nonequilibrium molecular dynamics (NEMD) method is employed to calculate the thermal conductivity, and the equations of atom motion are integrated with a time step of  $1.0 \text{ fs}$ . Periodic boundary conditions are applied in all three directions. The initial system is firstly relaxed in the constant pressure and constant temperature (NPT) ensemble for  $500 \text{ ps}$  at a designated temperature and the pressure of  $0 \text{ bar}$ , subsequently switched to a constant volume and constant temperature (NVT) ensemble for  $200 \text{ ps}$  for further relaxation. In the following, the microcanonical ensemble (NVE) is applied to the system to obtain converged energy of the whole system. Meanwhile, heat flux  $J$  is introduced by continuously adding and removing energy in the thermostated regions at an energy exchange rate  $dE/dt = 0.3 \text{ eV ps}^{-1}$ , which can be expressed as following:

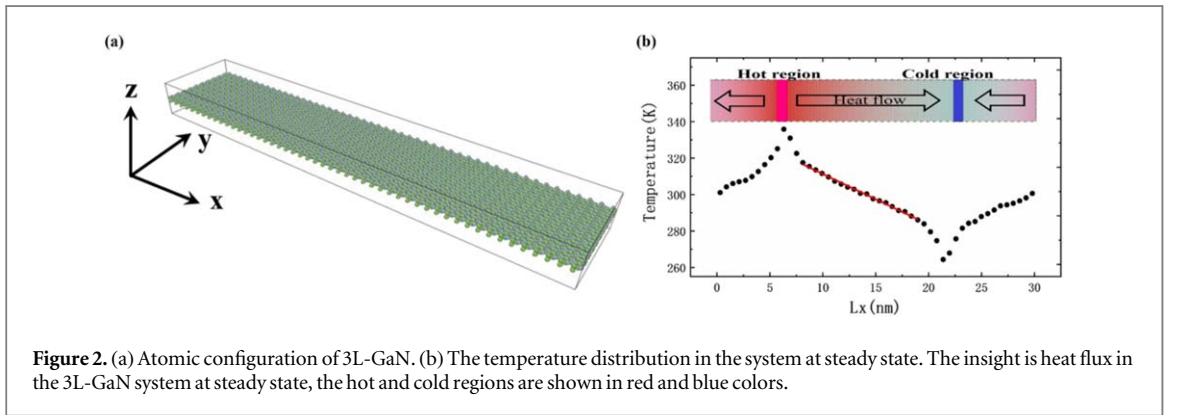
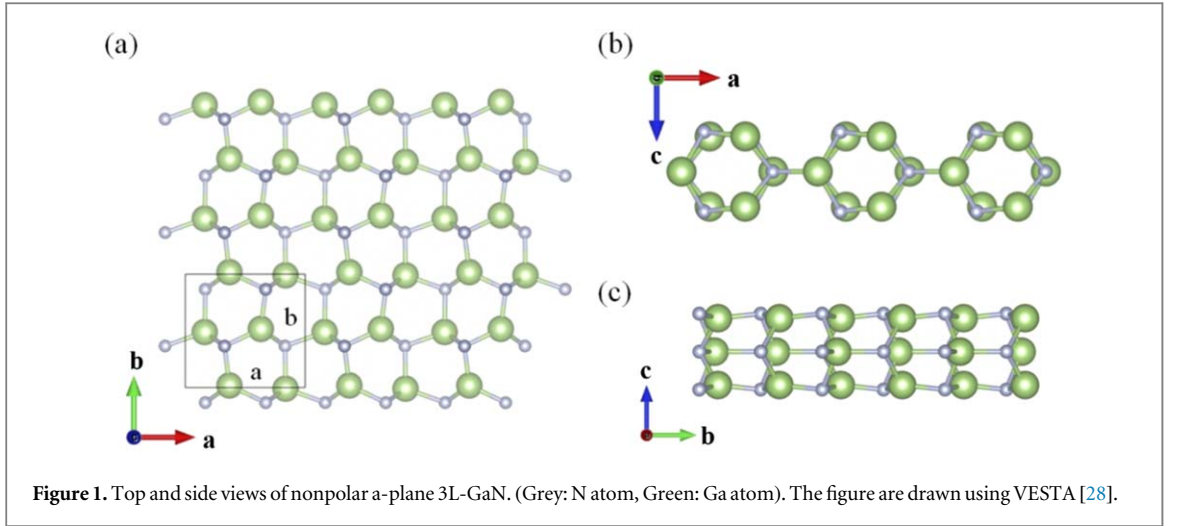
$$J = \frac{dE/dt}{A} \quad (1)$$

where  $A$  is the cross-sectional area of the simulation system in the direction perpendicular to heat transport. The temperature gradient between hot and cold regions is established after  $1 \text{ ns}$  when the system reached a steady state as shown in figure 2(b). The thermal conductivity  $\kappa$  of 3L-GaN from the NEMD simulations can be calculated according to the Fourier's law:

$$\kappa = \frac{J}{\partial T/\partial L} \quad (2)$$

where  $J$  is the heat flux mentioned above and  $\partial T/\partial L$  is the temperature gradient along the heat flux direction, which is the slope of the linear fitting of temperature distribution as the red line shown in figure 2(b). The linear fitting slope  $\partial T/\partial L$  is in a range  $\partial T/\partial L \pm \varepsilon$  due to the temperature fluctuation. As a result, the accuracy of thermal conductivity is also affected. The error bar is the maximum difference of the thermal conductivity calculating from  $\partial T/\partial L \pm \varepsilon$  and  $\partial T/\partial L$ .

In order to gain a deeper understanding of the thermal transport properties, the phonon density of state (PDOS) is calculated. After the simulation system is fully relaxed in the NPT and NVT ensemble, the PDOS is computed in the NVE ensemble from the Fourier transform [32] of the velocity-velocity autocorrelation



function (VACF) of atoms as:

$$P(\omega) = \frac{1}{\sqrt{2\pi}} \int_0^{\tau} \langle v(t) \cdot v(0) e^{-i\omega t} \rangle dt \quad (3)$$

where  $P(\omega)$  denotes the density of state at frequency  $\omega$  and  $\langle v(t) \cdot v(0) \rangle$  is the correlation function of ensemble average which replaces time average. In our work, the velocity is computed every 5 fs with a total integration time of 15 ps.

### 3. Results and discussion

#### 3.1. In-plane thermal conductivities

As the system size has a significant effect on the thermal properties due to the phonon boundary scattering, the finite size effect must be taken into account. To obtain the thermal conductivity  $\kappa$  of the infinite-size for a-plane 3L-GaN, we have investigated the thermal conductivity in both the zigzag and armchair directions.

The width effect test shown in figure S1 in the supplementary material indicates that a width of 10 unitcell (5.2 nm) has converged. Therefore, in the following calculation of thermal conductivity along the armchair direction (length 30.1 ~ 223 nm) and zigzag direction (length 26.3 ~ 210.7 nm), the widths are both set to 5.2nm. The length-dependent thermal conductivity with the error bar along zigzag- and armchair-direction of 3L-GaN is shown in figure 3(a) and a linear fit procedure is used to get the thermal conductivity at the infinity:

$$\frac{1}{\kappa} = \frac{1}{\kappa_{\infty}} \left( \frac{4L}{l} + 1 \right) \quad (4)$$

where  $\kappa_{\infty}$  is the thermal conductivity of infinite length,  $L$  is the effective phonon mean free path, and factor 4 represents a quarter of the total length which is the average distance of phonon scattering in the NEMD process as shown in figure 2. The fitted thermal conductivity of the 3L-GaN along zigzag- and armchair-direction is  $70.22 \text{ Wm}^{-1}\text{K}^{-1}$  and  $41.81 \text{ Wm}^{-1}\text{K}^{-1}$  respectively as shown in figure 3(b). The anisotropy of the thermal conductivity of a-plane GaN reinforces the prospective application in the construction of photonic devices.

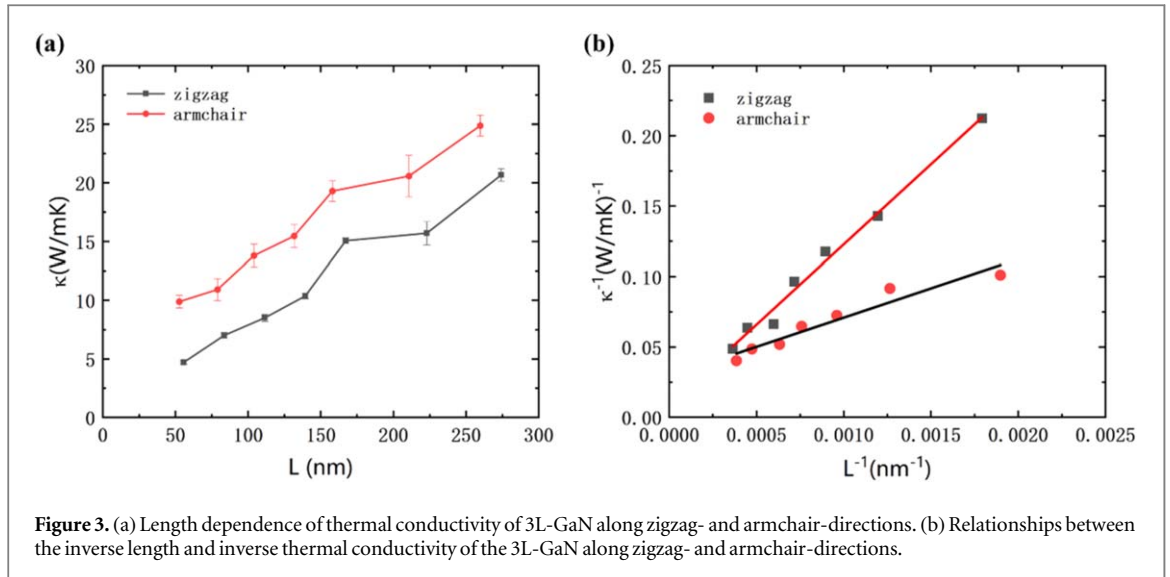


**Figure 3.** (a) Length dependence of thermal conductivity of 3L-GaN along zigzag- and armchair-directions. (b) Relationships between the inverse length and inverse thermal conductivity of the 3L-GaN along zigzag- and armchair-directions.

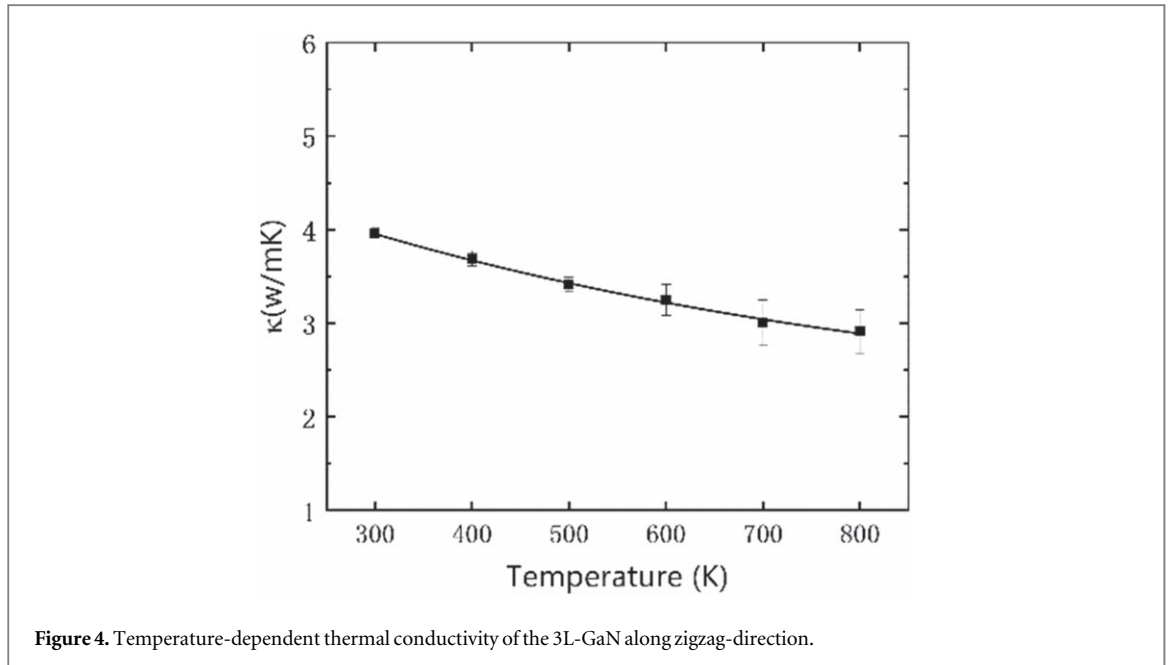


**Figure 4.** Temperature-dependent thermal conductivity of the 3L-GaN along zigzag-direction.

Since the conductivity along the zigzag-direction is larger, we are interested in the tunability of the thermal conductivity in this direction in the following.

### 3.2. Temperature effect

In reality, nanodevices in practical applications can be used in different tough conditions including various high working temperatures, which can affect their thermal conductivity. In this section, we have explored the temperature-dependent thermal conductivity of 3L-GaN at temperatures ranging from 300 K to 800 K. Instead of putting emphasis on the absolute values of thermal conductivity, we are interested in the tendency of the thermal conductivity at varying temperatures. Thus, the system with a length of 55.7 nm (along zigzag-direction) and a width of 5.2 nm (armchair-direction) is selected to illustrate the temperature effect on thermal conductivity without considering the size effect in the following research. As shown in figure 4, the thermal conductivity of 3L-GaN decreases monotonically as the temperature increase. This phenomenon is in accordance with a phonon-dominated crystalline material [33]. At high temperature, more phonon with high frequency will be activated and participate in thermal transport; however, the rising temperature facilitates Umklapp scattering on the other hand, and thus in turn suppresses phonon transport. These two effects compete with each other, and the Umklapp phonon scattering effect plays a dominant role in thermal transport, which leads to a decrease in thermal conductivity.

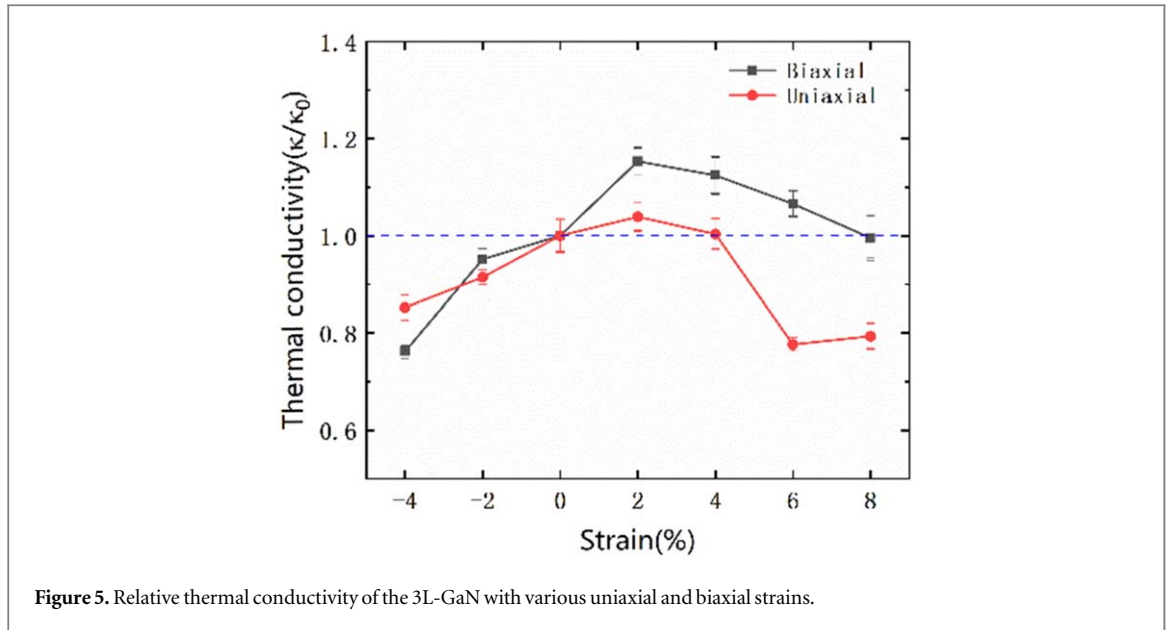


Figure 5. Relative thermal conductivity of the 3L-GaN with various uniaxial and biaxial strains.

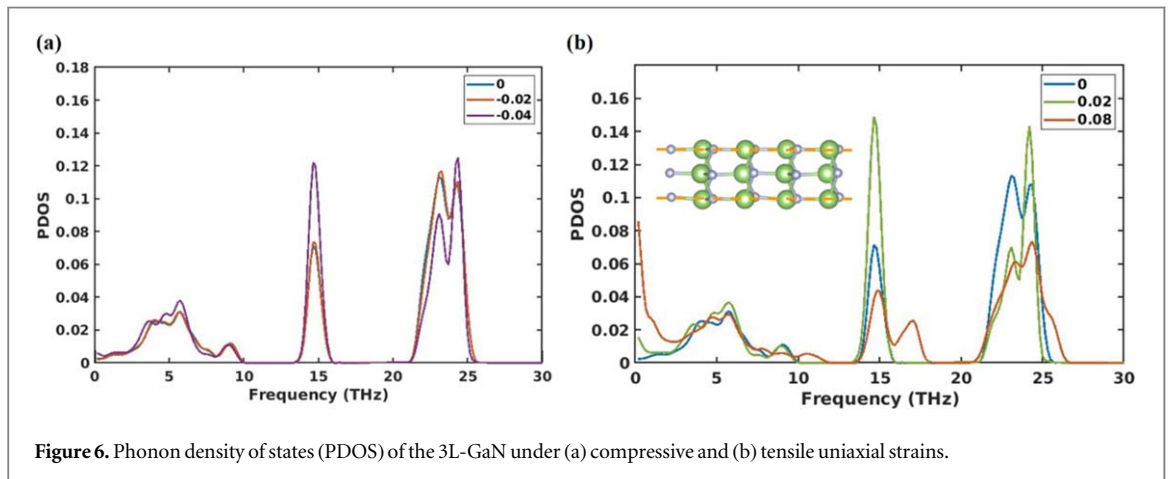


Figure 6. Phonon density of states (PDOS) of the 3L-GaN under (a) compressive and (b) tensile uniaxial strains.

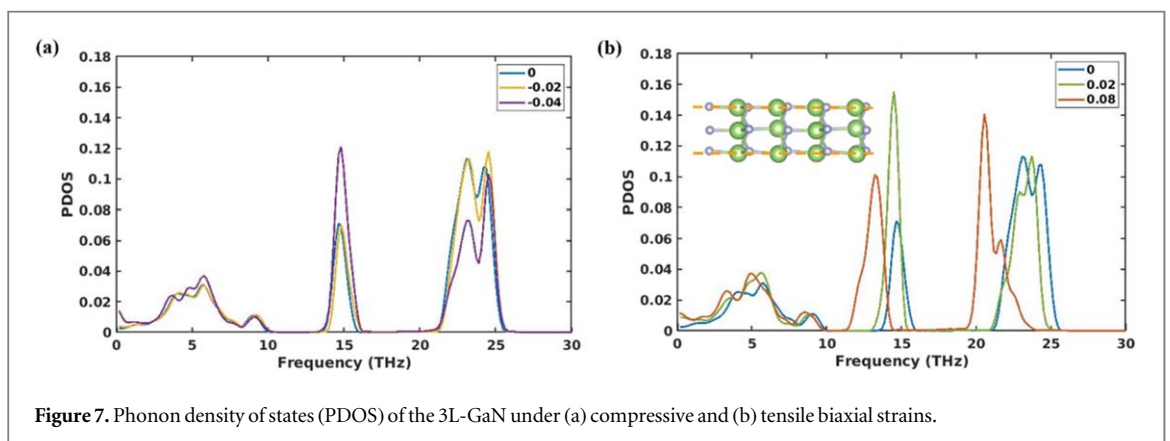


Figure 7. Phonon density of states (PDOS) of the 3L-GaN under (a) compressive and (b) tensile biaxial strains.

### 3.3. Strain effect

#### 3.3.1. Uniaxial strain effect

To further enrich the potential application scenarios of 2D materials and broaden their scope of application, it is of great significance to modulate their thermal transport properties. As confirmed by numerous studies, various approaches have been successfully achieved, and engineering (mechanical) strain is one of the efficient ways to tune thermal transport properties of nanomaterials. In addition, strain can be easily introduced both in the fabrication and working process [34]. To comprehensively understand the thermal properties of 3L-GaN, the effects of strain on thermal conductivity are investigated. The strain is defined as

$$\varepsilon = \frac{l - l_0}{l_0} \quad (5)$$

where  $l_0$  and  $l$  are the length of the simulation box along the strain loading direction for the strain-free and strained system. The  $\varepsilon > 0$  and  $\varepsilon < 0$  represent tensile strain and compressive strain applied respectively. After the system reaches its equilibrium, a constant strain rate of  $1.0 \times 10^8 \text{ s}^{-1}$  is applied in the longitudinal (zigzag) direction. In this work, uniaxial strain ranging from  $-0.04$  (compression) to  $0.08$  (tension) is applied to the system. The calculated relative thermal conductivity of 3L-GaN under uniaxial strains is shown in figure 5, which is normalized by the corresponding values of the strain-free system.

As shown in figure 5, the relative thermal conductivity gradually decreases with the increasing compressive strain, indicating that compressive strain has a non-negligible effect on the thermal conductivity of the system. This phenomenon is consistent with graphite carbon nitride but differs with multi-layer graphene [22]. To have a better understanding of the trend, the PDOS under variable compressive strains of the system is calculated and shown in figure 6(a). In the overall domain, we find that the curves of unstrained and compressed 0.02 strain almost overlap with each other except a small shift on high-frequency, suggesting that the decrease of the thermal conductivity of the system is attributed to the peak shift. At larger compressed strain, the peak of high-frequency ( $> 20 \text{ THz}$ ) decreases while the peaks at low- and intermediate-frequency regions are enhanced, suggesting that the decrease of thermal conductivity is resulted from enhanced phonon scattering.

When uniaxial tensile strain is applied, the thermal conductivity slightly increases with strain up to 0.02 and then decreases in the range from 0.02 to 0.08. It is worth noting that the tendency of the up-then-down thermal conductivity under uniaxial tensile strain is consistent with the results of other materials in previous studies [22, 24–26]. The small increase in thermal conductivity is mainly attributed by the two factors: (a) the small tensile strain introduced into those materials can reduce wrinkles, which in turn reduces the phonon scattering caused by surface bending; (b) as shown in figure 6(b) that the introduced tensile strain causes the sharper peak at high frequency and reduces the phonon scattering. As the tensile strain increases further, a decreasing trend of the relative thermal conductivity curve resulted from the softening of high-frequency peaks and broadening of the width can be found. The increased phonon scattering plays a domain role during the decrease of thermal conductivity according to the classical lattice thermal transport theory [35].

### 3.3.2. Biaxial strain effect

In addition to the uniaxial strain, we also explore the effect of the biaxial strain on the thermal conductivity of the 3L-GaN. After the relaxation and equilibrium, a constant strain rate of  $1.0 \times 10^8 \text{ s}^{-1}$  is applied along both zigzag- and armchair- direction. We introduce the equivalent strain levels ranging from  $-0.04$  to  $0.08$  in both zigzag- and armchair- directions to the samples with a length of  $55.7 \text{ nm}$  (zigzag direction) and a width of  $5.2 \text{ nm}$  (armchair direction). The relative thermal conductivity along the heat flux direction is calculated according to the same method as that in the uniaxial strains mentioned above and normalized by the corresponding strain-free sample, shown in figure 5.

When varies biaxial compressive strains are applied to the system, similar to the effect of uniaxial compressive strain, the thermal conductivity decreased monotonically as the biaxial compressive strain increases. The variation of the PDOS with the compressive strain (figure 7(a)) is similar to that of uniaxial strain (figure 6(a)).

When biaxial tensile strain is applied, the thermal conductivity shows an up-then-down behavior and reaches the maximum at strain of 0.02. It could be understood from PDOS shown in figure 7(b). At small tensile strain of 0.02, the peak at high frequency increases and the width decreases a little bit, indicating the decrease of both the phonon scattering and the group velocity at high frequency. However, at large tensile strain of 0.08, there is an obvious red shift of the peak in the whole region, indicating a significant phonon-phonon scattering and resulting in a decrease of the thermal conductivity. The peak values and positions have distinct responses to the strain, causing the up-then-down thermal conductivity of 3L-GaN.

Compared with the uniaxial strain, the tunability of the thermal conductivity by biaxial strain is much larger. The maximum change in the thermal conductivity is 22% by biaxial tensile strain while it is merely enhanced 3% by uniaxial tensile strain.

## 4. Conclusion

In this work, we investigate the thermal conductivity of the nonpolar a-plane 3L-GaN based on the non-equilibrium molecular dynamic simulation and explored the effect of temperature, biaxial and uniaxial strain on the thermal conductivity. It is found that there is an in-plane thermal anisotropy in the nonpolar 3L a-plane GaN, with the thermal conductivities for the infinite-length 3L-GaN at room temperature along zigzag- and armchair-directions are predicted to be  $70.22 \text{ W m}^{-1} \text{ K}^{-1}$  and  $41.81 \text{ W m}^{-1} \text{ K}^{-1}$  respectively. Moreover, the

decrease trend between the thermal conductivity and temperature is also predicted, which is consistent with other materials. In addition, we find that the thermal conductivity of GaN trilayer can be effectively modulated by strain and the biaxial strain tunability is much larger than that of uniaxial. The understanding on thermal transport properties of nonpolar a-plane GaN will facilitate further study on a-plane gallium nitride and promote its potential application in thermal management and nanodevices.

It should be noted that the SW potential is usually used in the bulk GaN and the phonon dispersion comparison with the density functional theory (DFT) (Supplementary material S6) indicate that the current potential could be improved. Machine-learning interatomic potentials [36, 37] is a promising method that has DFT accuracy and MD efficiency. We will consider this method in the future research.

## Acknowledgments

D.X. acknowledges support from the National Natural Science Foundation of China (No. 51806072). And helpful discussions with Professor Nuo Yang and Dr Xiao Wang are acknowledged.

## Data availability statement

All data that support the findings of this study are included within the article (and any supplementary files).

## ORCID iDs

Dongwei Xu  <https://orcid.org/0000-0002-5847-3711>

Xiaobing Luo  <https://orcid.org/0000-0002-6423-9868>

## References

- [1] Nakamura S *et al* 2013 History of gallium–nitride-based light-emitting diodes for illumination *Proc. IEEE* **101** 2211–20
- [2] DenBaars S P *et al* 2013 Development of gallium-nitride-based light-emitting diodes (LEDs) and laser diodes for energy-efficient lighting and displays *Acta Mater.* **61** 945–51
- [3] Chen Y X *et al* 2019 GaN in different dimensionalities: properties, synthesis, and applications *Materials Science & Engineering R-Reports*. **138** 60–84
- [4] Hu L *et al* 2020 High-power hybrid GaN-based green laser diodes with ITO cladding layer *Photonics Research* **8** 279–285
- [5] Qin Z Z *et al* 2017 Orbitally driven low thermal conductivity of monolayer gallium nitride (GaN) with planar honeycomb structure: a comparative study *Nanoscale*. **9** 4295–309
- [6] Neufeld C J *et al* 2008 High quantum efficiency InGaN/GaN solar cells with 2.95 eV band gap *Appl. Phys. Lett.* **93** 143502
- [7] Ganguly S *et al* 2012 Polarization effects on gate leakage in InAlN/AlN/GaN high-electron-mobility transistors *Appl. Phys. Lett.* **101** 253519
- [8] Baxter J *et al* 2009 Nanoscale design to enable the revolution in renewable energy *Energy Environ. Sci.* **2** 559–88
- [9] Cai X R *et al* 2020 Strain-induced phase transition and giant piezoelectricity in monolayer tellurene *Nanoscale*. **12** 167–72
- [10] Wang Q H *et al* 2012 Electronics and optoelectronics of two-dimensional transition metal dichalcogenides *Nat. Nanotechnol.* **7** 699–712
- [11] Ng T Y *et al* 2012 A molecular dynamics study of the thermal conductivity of graphene nanoribbons containing dispersed Stone–Thrower–Wales defects *Carbon* **50** 4887–93
- [12] Novoselov K S *et al* 2012 A roadmap for graphene *Nature* **490** 192–200
- [13] Wang X Y *et al* 2017 Molecular dynamics study of thermal transport in a nitrogenated holey graphene bilayer *J. Mater. Chem. C* **5** 5119–27
- [14] Novoselov K S *et al* 2004 Electric field effect in atomically thin carbon films *Science* **306** 666–9
- [15] Qin G Z *et al* 2017 Anomalously temperature-dependent thermal conductivity of monolayer GaN with large deviations from the traditional  $1/T$  law *Phys. Rev. B* **95** 195416
- [16] Mu Y W 2015 Chemical functionalization of GaN Mono layer by adatom adsorption *J. Phys. Chem. C* **119** 20911–6
- [17] Shu H B *et al* 2019 Effects of strain and surface modification on stability, electronic and optical properties of GaN monolayer *Appl. Surf. Sci.* **479** 475–81
- [18] Cai X R *et al* 2021 Effect of hydrogenation on the thermal conductivity of 2D gallium nitride *Phys. Chem. Chem. Phys.* **23** 22423–9
- [19] Cai X R *et al* 2021 Structure and electronic bandgap tunability of m-plane GaN multilayers *Phys. Chem. Chem. Phys.* **23** 5431–7
- [20] Kolobov A V *et al* 2017 Strain engineering of atomic and electronic structures of few-monolayer-thick GaN *Phys. Rev. Materials*. **1** 024003
- [21] Kolobov A V *et al* 2016 Instability and spontaneous reconstruction of few-monolayer thick GaN graphitic structures *Nano Lett.* **16** 4849–56
- [22] Song J R *et al* 2020 Thermal transport properties of graphite carbon nitride *Phys. Chem. Chem. Phys.* **22** 22785–95
- [23] Hong Y *et al* 2018 Monolayer and bilayer polyaniline C<sub>3</sub>N: two-dimensional semiconductors with high thermal conductivity *Nanoscale*. **10** 4301–10
- [24] Zhang Y Y *et al* 2017 Thermal conductivity of a h-BCN monolayer *Phys. Chem. Chem. Phys.* **19** 27326–31
- [25] Song J R *et al* 2019 Thermal conductivity of two-dimensional BC<sub>3</sub>: a comparative study with two-dimensional C<sub>3</sub>N *Phys. Chem. Chem. Phys.* **21** 12977–85
- [26] Lin C P *et al* 2017 Theoretical prediction of thermal transport in BC<sub>2</sub>N monolayer *Nano Energy*. **38** 249–56



- [27] Ding B *et al* 2021 Anomalous strain effect on the thermal conductivity of low-buckled two-dimensional silicene *Natl Sci. Rev.* **8** [nwaa220](#)
- [28] Momma K 2011 VESTA 3 for three-dimensional visualization of crystal, volumetric and morphology data *J. Appl. Crystallogr.* **44** [1272–6](#)
- [29] Rezaee F *et al* 2021 Heat transfer in strained twin graphene: A non-equilibrium molecular dynamics simulation *Physica A* **564** [125542](#)
- [30] Plimpton S 1995 Fast parallel algorithms for short-range molecular dynamics *J. Comput. Phys.* **117** [1–19](#)
- [31] Béré A *et al* 2006 On the atomic structures, mobility and interactions of extended defects in GaN: dislocations, tilt and twin boundaries *Philos. Mag.* **86** [2159–92](#)
- [32] Dickey J M *et al* 1969 Computer simulation of the lattice dynamics of solids *Phys. Rev.* **188** [1407](#)
- [33] Liang T *et al* 2019 A molecular dynamics study on the thermal conductivities of single- and multi-layer two-dimensional borophene *Nano Futures* **3** [015001](#)
- [34] Mayelifartash A *et al* 2021 Thermal conductivity and interfacial thermal resistance behavior for the polyaniline-boron carbide heterostructure *Phys. Chem. Chem. Phys.* **23** [13310–22](#)
- [35] Wei N *et al* 2011 Strain engineering of thermal conductivity in graphene sheets and nanoribbons: a demonstration of magic flexibility *Nanotechnology* **22** [105705](#)
- [36] Mortazavi B *et al* 2021 Accelerating first-principles estimation of thermal conductivity by machine-learning interatomic potentials: a MTP/ShengBTE solution *Comput. Phys. Commun.* **258** [107583](#)
- [37] Mortazavi B *et al* 2021 Exceptional piezoelectricity, high thermal conductivity and stiffness and promising photocatalysis in two-dimensional MoSi<sub>2</sub>N<sub>4</sub> family confirmed by first-principles *Nano Energy*. **82** [105716](#)